C. Chiquete, S.I. Jackson and M. Short.
"DSD calibration of PBX 9501 via slab geometry experiments."
In Proceedings of the 15th International Detonation Symposium, Office of Naval Research, pp. 494-503 (Office of Naval Research, 2015).

DSD calibration of PBX 9501 via slab geometry experiments

Carlos Chiquete[1], Scott I. Jackson[1] and Mark Short[1]

[1]Shock and Detonation Physics Group, Weapons Experiments Division, Los Alamos National Laboratory, Los Alamos, NM 87545

Abstract. The Detonation Shock Dynamics (DSD) calibration for the plastic-bonded explosive PBX 9501 is revisited, incorporating recent slab geometry tests conducted by Jackson and Short[1]. To address the question of which geometry (slab or rate-stick) may be preferable for calibration, we will present a series of PBX 9501 DSD calibrations obtained using only detonation phase velocity and front shape measurements extracted from the slab geometry tests for a number of $D_n(\kappa)$ functional forms. The corresponding predictions of the diameter effect curves are then compared to the available data. Calculations of the thickness effect curve and slab front shapes from a previously obtained PBX 9501 DSD calibration by Aslam[2] (based on cylindrical rate-stick experiments with two front shapes obtained for a single charge-diameter) are, in turn, compared to the new slab geometry test data. The compatibility of the two data sets for DSD calibration of PBX 9501 is evaluated and discussed.

Introduction

To efficiently calculate the timing and energy delivery of a detonating explosive in a complex engineering geometry, Programmed Burn (PB) strategies[3, 4] have been developed to circumvent the numerical difficulties that arise from the large scale disparity between the explosive's reaction zone width and the much larger geometric engineering length and time scales in a full continuum simulation. PB methods separate calculations of the timing of the detonation propagation through the explosive geometry from the energy delivery calculation. The Detonation Shock Dynamics (DSD) modeling methodology[5, 6, 7, 8] is a central aspect for the timing component of modern PB approaches, replacing the detonation front and reaction zone with a propagated surface evolved according to a specified propagation law, in which the normal detonation velocity D_n is a function of the local surface curvature κ. The theory is based on the assumption of quasi-steady propagation of the front and small detonation front curvature with respect to the reaction zone time and length scales[5]. Applying level set techniques[9] and an established $D_n-\kappa$ law, the detonation front surface can then be propagated throughout a complex three-dimensional geometry providing accurate time-of-arrival predictions at any point in the geometry. The confining material effect is incorporated within the theory by specification of the shock angle ϕ_e at the interface between the explosive and inert confining material. In most cases, the propagation law is obtained using experimental data involving diameter effect points and detonation

Approved for unlimited release: LA-UR-14-24744

front shapes in a rate-stick configuration[10]. A key question is then, how calibrations obtained from the more recently developed slab geometry tests compare to the conventional rate-stick approach.

In the present work, the newly performed slab geometry calibration tests are used to calibrate the PBX 9501 $D_n - \kappa$ relation (for various functional forms). PBX 9501 is a polymer bonded explosive composed of 95.0 weight (wt.) % HMX explosive crystals bonded with a binder mixture of 2.5 wt. % Estane and a 2.5 wt. % eutectic mixture of bis(2,2-dinitropropyl)acetal and bis(2,2-dinitropropyl)formal (BDNPA/BDNPF). PBX 9501 is considered to be a conventional (or ideal) high explosive with a small reaction zone length scale of $\mathcal{O}(100\,\mu\text{m})$, a nominal detonation velocity of 8.8 mm/μs, and a failure charge-radius near 0.76 mm[11]. The resulting calibrations are used to calculate diameter effect curves, which are then compared to the corresponding experimental data originating from the rate-stick tests. A previously obtained calibration of PBX 9501 by Aslam[2] which was based solely on data extracted from rate-stick tests is, in turn, used to calculate a thickness effect curve and compared to the experiments. The results of these comparisons are discussed in terms of the ability of the DSD calibration methodology to capture the complete set of data across the two test geometries.

PBX 9501 Slab Experiments

Slab geometry experiments are designed to generate a region of quasi-steady, two dimensional flow along the centerline of the explosive. This allows the measurement of both detonation phase velocities and detonation front shapes at the breakout surface within this region. The explosive slabs in the current study were unconfined as in the previous PBX 9501 rate-stick calibration experiments.

Eight slab tests were performed by Jackson and Short[1] with the PBX 9501 formulation. The slab experiments were boosted with a line wave generator composed of XTX-8003 (80% PETN and 20% silicone resin, specifically Sylgard 182 elastomer). The PBX 9501 main charges were approximately 130 mm in length and 150 mm in width with thicknesses varying from 0.8–8.0 mm. Slab densities were in the range 1.8295-1.8334 g/cc. The phase velocity of

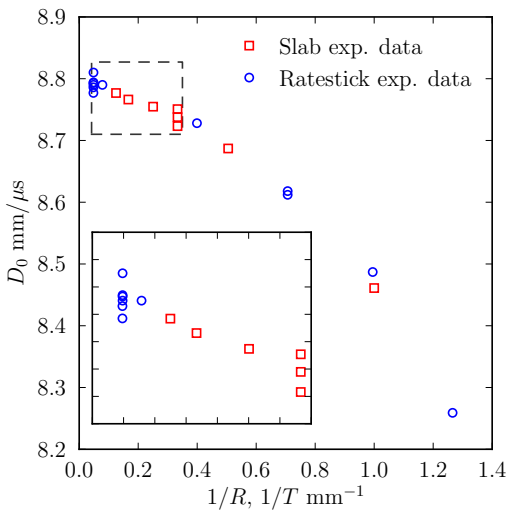

Fig. 1. Size-effect data for PBX 9501. Blue circles ◯ and red squares □ denote experimental slab and cylindrical rate stick detonation velocities, respectively (a convention adopted throughout). The insert on the lower left is the detail indicated by the dashed rectangle near D_{CJ}.

the detonation along the charge centerline was obtained through time-of-arrival (TOA) wires, where a least-squares linear fit to the measured TOA wire position and detonation arrival time produced the phase detonation phase speed (D_0). The standard errors associated with the linear fits were uniformly less than 0.006 mm/μs or about 0.07% the steady phase velocity in relative terms. Note that 6 front shapes were extracted from these tests (all at different charge-thicknesses).

For comparison with a different geometry, the equivalent rate-stick data set for PBX 9501 consists of a total of 12 diameter effect points and 2 front shapes at a single charge-diameter[12]. The diameter and thickness effect data is plotted in fig. 1. The horizontal axis is the inverse charge radius $1/R$ for the rate-stick geometry and the inverse slab thickness $1/T$ for the slab geometry.

Front curvature analysis

The detonation front shapes across the slab short-axis were digitized for the 1.00, 1.98, 3.00, 3.99,

6.00 and 8.01 mm thickness tests for a total of 6 data sets. The necessary vertical and horizontal scaling factors to extract the physical front shapes were determined from the detonation phase velocity, streak camera write speed and a pre-shot imaged fiducial.

To determine a representation of the normal velocity-curvature relation, the experimental front shapes were fit to a form used by Hill[13]. This is a series function form given by

$$z(r) = -\sum_{i=1}^{n} a_i \left[\ln\left(\cos\left(\frac{\pi\eta}{2R}r\right)\right)\right]^i, \qquad (1)$$

where r is the distance from the center and the parameters a_i and η ($0 < \eta < 1$) are fitting constants. Here, either $n = 1$ or $n = 2$ was chosen for fitting the slab front shape data to get a similar residual level for all fits.

Parameteric $D_n - \kappa$ data

The slab normal velocity D_n and the front curvature κ are found from the relations,

$$D_n = \frac{D_0}{\sqrt{1+(z')^2}}, \; \kappa = \frac{z''}{[1+(z')^2]^{3/2}} \qquad (2)$$

where $z' = dz/dr$, $z'' = d^2z/dr^2$. Use of a twice continuously-differentiable ($\mathcal{C}^2$) analytic function for $z(r)$ yields smooth values of the first and second derivatives ($z'(r)$ and $z''(r)$).

Analytic shock shapes of the form (1) were fitted to the raw experimental data for each test and are shown in fig. 2. Note the significant local scatter in the experimental shock shape due to the heterogenous nature of the PBX 9501 explosive with HMX grain sizes on the order of 100 μm[14]. The $D_n - \kappa$ relation derived for each test by using (2) is shown in fig. 3. For charge sizes of 1.98 mm and above, the $D_n - \kappa$ curves overlap well up to 90% of the charge thickness, while there is some divergence beyond 90% (for about $\kappa < 1.2$ mm^{-1}). For the 1 mm charge thickness, there is significantly more $D_n - \kappa$ variation over 90% of the charge thickness than for charge sizes 1.98 mm and above, and this is associated with the increased curvatures that are induced across the front for small charges.

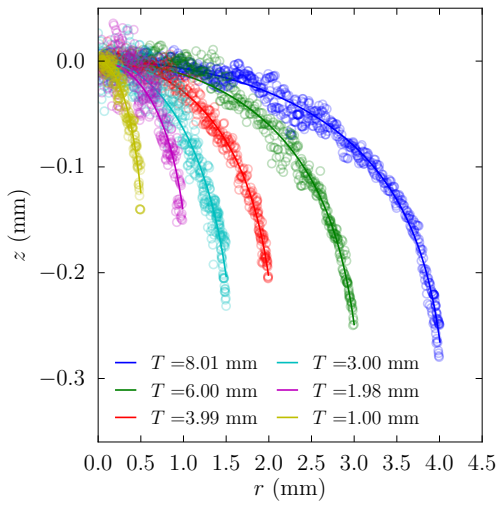

Fig. 2. Comparison of the shock shape log-form fits (eqn. (1)) to experimentally imaged shock shape data for each slab test.

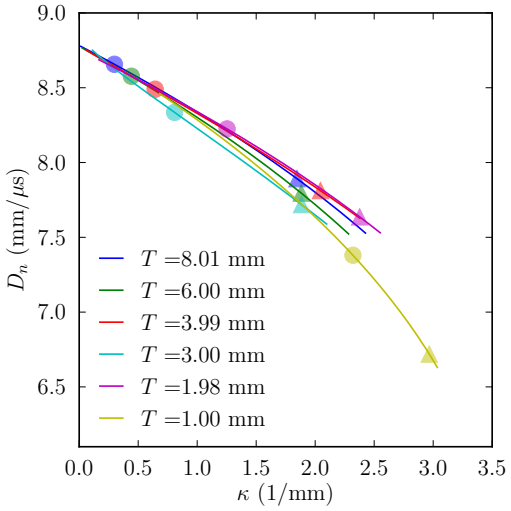

Fig. 3. The $D_n - \kappa$ data derived from eqns. (1) and (2) for each slab thickness. Circles represent the $D_n - \kappa$ variation up to 90% of the charge thickness, while the triangles denote 99% of the same measure.

DSD calibrations of slab data

To calibrate an explosive for DSD, a functional form for the $D_n - \kappa$ relation must be specified and its parameters systematically varied to optimally fit the available experimental data within the calibration procedure.

The calibration procedure used here is based on the approach of Bdzil et al.[15]. To quantify the quality of a particular fit, a merit function is defined that incorporates the error in the DSD-calculated detonation thickness effect currve and associated front shapes into a single metric. The merit function used here is,

$$\mathcal{M} = \frac{w}{N_{TE}} \sum_{i=1,N_{TE}} (F_i(D_{0,i}^{calc} - D_{0,i}^{exp}))^2 + \frac{1-w}{N_r^T} \sum_{i=1,N_{FS}} E_i \sum_{j=1,N_r^i} ((\boldsymbol{z}_j^{i,calc} - \boldsymbol{z}_j^{i,exp}))^2, \tag{3}$$

where $\boldsymbol{z}_j^{i,calc}$ and $\boldsymbol{z}_j^{i,exp}$ represent the calculated and experimental j-th shock shape point for the i-th test, $D_{0,i}^{calc}$ and $D_{0,i}^{exp}$ are the calculated and experimental detonation velocity for the i-th test, N_{TE} is the number of thickness effect points, N_r^i is the total number of shock front coordinates for the i-th test, $N_r^T = \sum_{i=1..N_{FS}} N_r^i$ is the total number of front shape coordinate points, and N_{FS} is the number of tests for which front shape data was obtained.

The merit function is structured with separate thickness effect and front shape error components. The factors E_i and F_i serve to nondimensionalize each error's contribution to the merit function. Here, the thickness effect and front shape errors were scaled with the experimental detonation velocity and the charge-half-width of each test, respectively. The relative contribution between the two sets of errors is determined by the parameter w. In the calibrations described below, w was set to 0.76, slightly favoring a reduction in the thickness effect error. The optimized parameters or parameterization of the $D_n - \kappa$ relation is obtained by numerically minimizing the defined multivariable merit function.

In the following, we present calibrations of the thickness effect data and the associated front shapes. The variations were obtained from calibrating three separate $D_n - \kappa$ functional forms. In all cases, the Chapman-Jouguet speed D_{CJ} and the edge angle ϕ_e were fixed in the optimization.

Rational polynomial form

The following standard $D_n - \kappa$ functional form is a polynomial in κ, given by

$$\frac{D_n}{D_{CJ}} = 1 - \alpha_1 \kappa \frac{1 + \alpha_2 \kappa + \alpha_3 \kappa^2}{1 + \alpha_4 \kappa + \alpha_5 \kappa^2}, \tag{4}$$

where the α_i are constants with $\alpha_i \geq 0$. The optimized parameters α_i along with fixed D_{CJ} and ϕ_e are given in table 1 (note that α_5 was not optimized and set to zero). The resulting global $D_n - \kappa$ curve is plotted in fig. 4 along with the log-form (1) derived $D_n - \kappa$ variation for each slab thickness. For smaller curvatures that cover 90% of the charge thickness, shown in the inset of fig. 4, the $D_n - \kappa$ variation derived from (4) follows the closely grouped log-form fits. For larger curvatures, the calibrated $D_n - \kappa$ curve does not follow the general concavity of the log-form fitted data while, for fixed D_n, it has a curvature toward the lower end of the majority of the log-form fitted experimental $D_n - \kappa$ data. This result is due to the influence of fitting the 1 mm thickness effect point (all thickness effect points had equal error bias), as it demanded a steep downturn in the calculated thickness effect curve to fit the 1 mm charge size, resulting in a comparatively large decrease in D_n as a function of κ.

Table 1. Optimized fit parameters for the rational polynomial $D_n - \kappa$ function.

Parameter	Values	Units
D_{CJ}	8.795	mm/μs
α_1	0.054	mm
α_2	2.415	mm
α_3	2.34×10^{-4}	mm^2
α_4	1.996	mm
α_5	0	mm^2
ϕ_e	29.86	deg

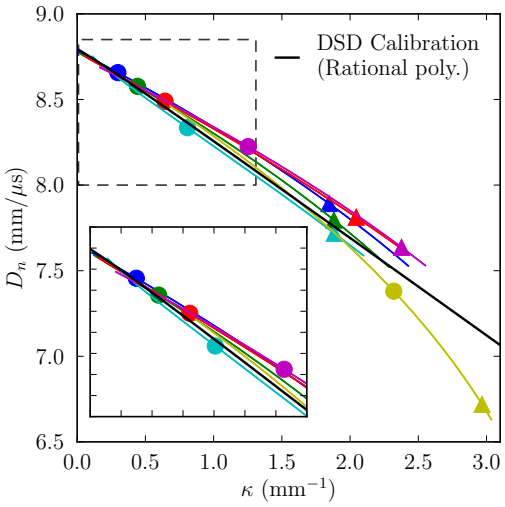

Fig. 4. The $D_n - \kappa$ variation from the optimized polynomial function form (eqn. (4)) (black line) compared with the various experimental log-form fits of the slab front shapes.

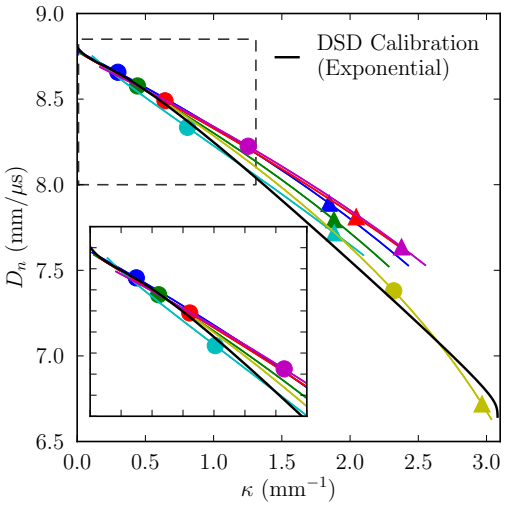

Fig. 5. The $D_n - \kappa$ variation from the optimized exponential function form (eqn. (5)) (black line) compared with the various experimental log-form fits of the slab front shapes.

Table 2. Optimized fit parameters for the exponential $D_n - \kappa$ function.

Parameter	Values	Units
D_{CJ}	8.803	mm/μs
α_1	0.119	mm
α_2	1.62×10^{-4}	mm
α_3	10.030	mm^2
α_4	5.652	mm
α_5	14.545	mm^2
A	0.037	mm^{e_1}
D_1	3.081	1/mm
e_1	0.075	
ϕ_e	28.98	deg

Exponential form

The following $D_n - \kappa$ functional form was also applied in the calibration of the slab data,

$$\frac{D_n}{D_{CJ}} = \left(1 + A((C_1 - \kappa)^{e_1} - C_1^{e_1}) - B\kappa \frac{1 + C_2\kappa + C_3\kappa^2}{1 + C_4\kappa + C_5\kappa^2}\right), \quad (5)$$

where A, e_1, C_1, B, C_2, C_3, C_4, and C_5 are the fitting parameters. Note that this is the form used in the previous DSD calibration of PBX 9501 by Aslam[2]. The result appears in fig. 5 and parameter values appear in table 2. When calibrated to the slab data, it was found that the contribution of the exponential term (which drives greater variation in D_n over a small span in κ) was relatively small in comparison to the results in Aslam[2]. This form captures the general concavity of the experimental $D_n - \kappa$ shapes. Up to 90% of the charge width (fig. 5 inset), the exponential form again captures the $D_n - \kappa$ variation well, but thereafter has too rapid a decrease in D_n as κ increases.

Fractional power form

Lastly, the $D_n - \kappa$ functional form

$$\frac{D_n}{D_{CJ}} = \left(1 - \frac{E\kappa^\gamma}{1 + \kappa^\beta}\right), \quad (6)$$

was calibrated to the slab data set, where E, γ, and β are the fitting parameters. The result of this calibration appears in fig. 6 and the parameters ap-

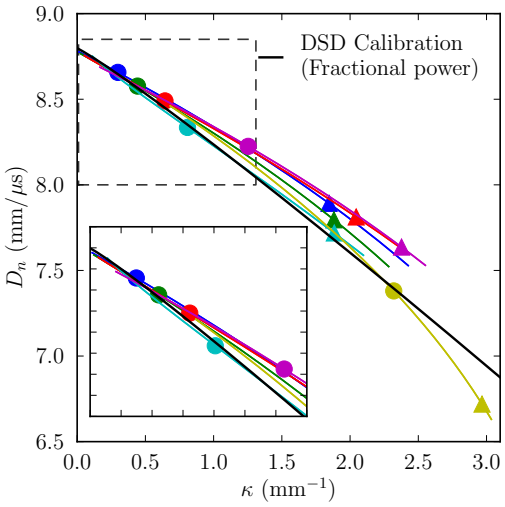

Fig. 6. The $D_n - \kappa$ variation from the optimized fractional power function form (eqn. (6)) (black line) compared with the various experimental log-form fits of the slab front shapes.

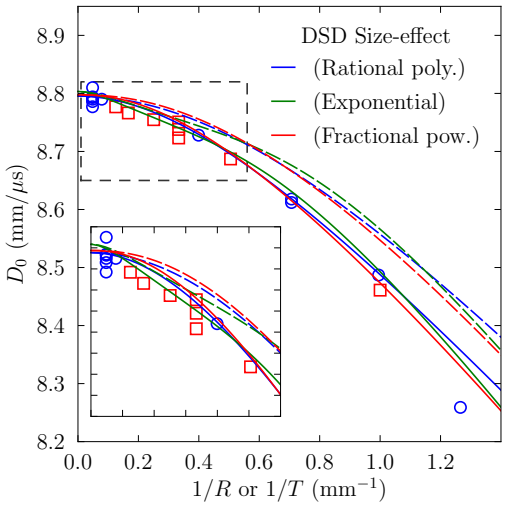

Fig. 7. The thickness effect curves (D_0 vs. $1/T$, solid lines) calculated from the three DSD calibrations (eqns. (4), (5) and (6)) shown against the experimental thickness effect data points (red squares). Also shown are the corresponding predictions of the diameter effect curves (D_0 vs. $1/R$, dashed lines) from the three DSD calibrations (eqns. (4), (5) and (6)) shown against the experimental diameter effect data points (blue circles).

pear in table 3. Again, we observe good agreement between the fitted $D_n - \kappa$ relation (6) and the $D_n - \kappa$ log-form fit to the experimental data that covers 90% of the charge width (inset to fig. 6). Thereafter the $D_n - \kappa$ fit (6) trends below the experimental data, again due to a balance between fitting shock shapes and thickness effect data.

Table 3. Optimized fit parameters for the fractional power $D_n - \kappa$ function.

Parameter	Values	Units
D_{CJ}	8.797	mm/μs
E	0.128	mm$^{\gamma}$
γ	1.087	
β	2.94×10^{-4}	
ϕ_e	29.60	deg

Slab thickness effect and shock shape comparison

Figure 7 shows the thickness effect curves (D_0 vs. $1/T$, solid lines) calculated from the three DSD calibrations (eqns. (4), (5) and (6)) shown against the experimental thickness effect data points (red squares). The residual level (in RMS) is on the order of the experimental velocity standard error for all the calibrated curves. The polynomial and fractional power fits slightly overestimate the thick effects points at large slab sizes (inset to fig. 7) due to the way the functional forms require a more rounded variation in $D_n - \kappa$ for small κ. Each of the calibrations also had a similar level of error in terms of the front shape data (for example, fig. 8 shows the results for the exponential $D_n(\kappa)$ function).

Comparing to the rate-stick data

One of the major benefits of a DSD formulation, where the normal detonation velocity is a function of the local shock curvature, is that its a geometry free representation. This implies that once a DSD relation is calibrated, in this case to the slab geometry, it should accurately capture detonation wave propagation timing in other geometries, such as cylindrical rate-sticks, provided that the nor-

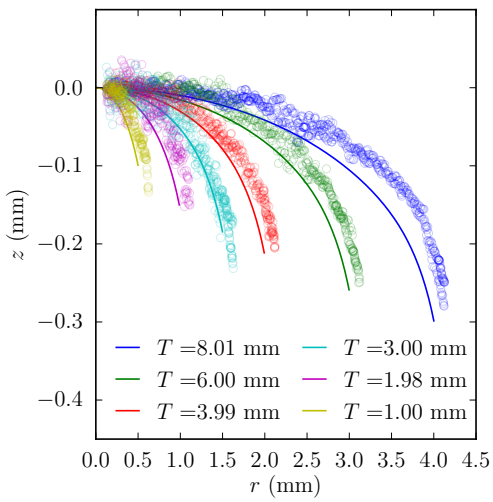

Fig. 8. The calculated front shapes for the exponential $D_n - \kappa$ functional form (5) compared to the experimental data.

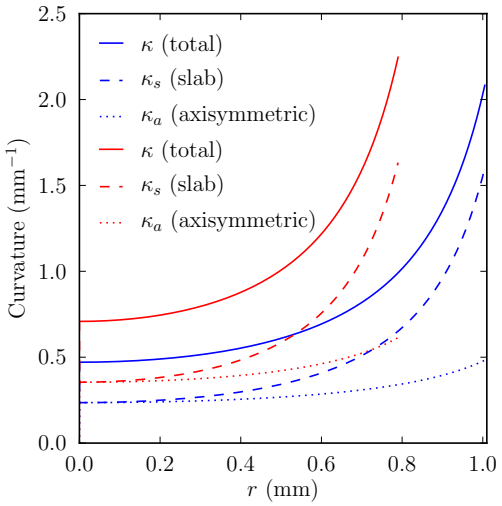

Fig. 9. The predicted total curvature along with the separate slab and axisymmetric curvatures components for rate-stick radii $R = 1.005$ mm (shown in blue) and $R = 0.79$ mm (shown in in red).

mal detonation curvature primarily depends on local curvature. This is the basis behind recent work on the geometry depend behavior of DSD for PBX 9501, PBX 9502 and ANFO by Jackson & Short[1]. In this regard, fig. 7 also shows the corresponding predictions of the diameter effect curves (D_0 vs. $1/R$, dashed lines) from the three DSD calibrations (eqns. (4), (5) and (6)) along with the experimental diameter effect data points (blue circles). It is clear that each DSD prediction for the diameter effect curve lies above the experimentally determined curve. In fact, the experimental data shows a size effect scale close to unity, i.e when $D_0(R) = D_0(T)$ and the ratio of charge radius R to the slab thickness T is close to unity. A similar issue in predicting the propagation in the alternative geometry was found by Jackson & Short[1] for the DSD prediction of the PBX 9501 thickness effect curve using a previous DSD calibration of PBX 9501 rate-stick data by Aslam[2].

On the other hand, Jackson & Short[1] found that for the more non-ideal HE PBX 9502, a DSD calibration based on the rate-stick geometry gives a good prediction of the experimentally determined thickness effect curve in the slab geometry. The reason the thickness effect curve (when plotted as D_0 vs. $1/T$) lies to the left of the diameter effect curve (when plotted as D_0 vs. $1/R$) can be seen by examining the resulting (slab and axisymmetric) curvature components. These components are plotted in fig. 9, calculated from the $D_n - \kappa$ slab-derived fit (5). For both rate-stick calculations shown at $R = 0.79$ and $R = 1.005$ mms, near the origin, the two curvature components are close in magnitude. Thereafter the slab curvature component grows in magnitude relative to the axisymmetric component. This difference in curvature component variations across the charge underlies the difference in the size effect curves shown in fig. 7, as previously explained by Jackson & Short[1]. For a $D_n - \kappa$ based DSD description to reproduce the observed experimental data which has a scale factor close to one, it would require the slab and axisymmetric curvature components to be equal across the charge[1].

Previous calibration of rate-stick data

Aslam[2] has previously determined a $D_n - \kappa$ relation for PBX 9501 based solely on calibration to rate-stick geometry experiments[12]. Figure 10 shows a comparison between the rate-stick cali-

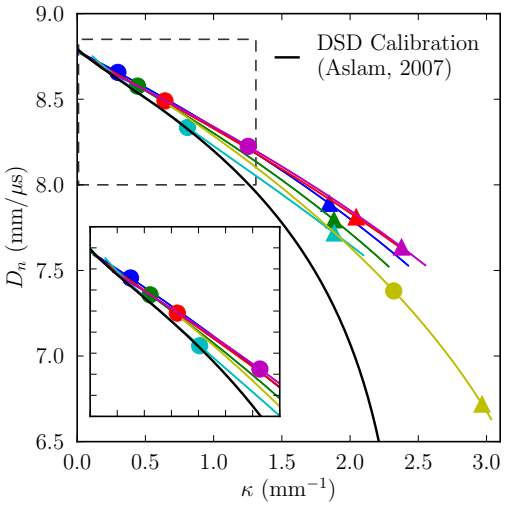

Fig. 10. The $D_n - \kappa$ function previously found by Aslam[2] compared to the various experimental log-form fits of the slab front shapes. Again, circles represent 90% of the radial extent of each front shape, and the triangle denotes 99% in the same measure.

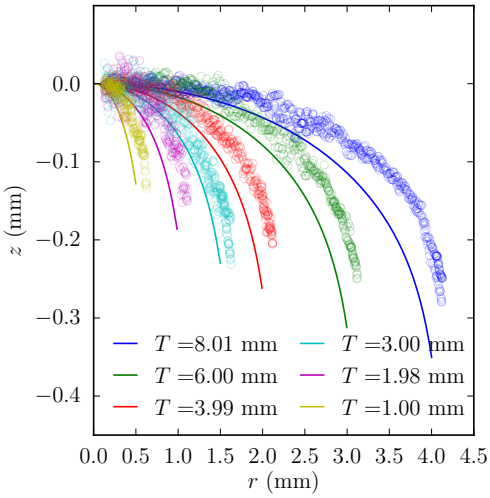

Fig. 11. The predicted front shapes by Aslam's[2] calibration of the rate-stick data compared to the experimental data.

brated $D_n - \kappa$ relation and the experimentally derived $D_n - \kappa$ curves for the slab geometry. It is seen that the $D_n - \kappa$ curve based on rate-stick geometry calibration has too rapid a decrease in D_n with increasing curvature to match the slab geometry data, even for small curvatures (as seen in the inset to fig. 10). Although the $D_n - \kappa$ relation derived by Aslam[12] fits the rate-stick diameter effect curve well, the more rapid decrease of D_n with κ would lead to smaller phase velocities in the slab geometry than observed experimentally, and again underlies the discrepancy in the size effect curves shown in fig. 7. In fig. 11, the slab shock shapes are compared with those predicted by the $D_n - \kappa$ relation derived by Aslam[2]. Again the $D_n - \kappa$ derived shapes are generally too curved to match the slab data.

Discussion

It is clear from the above that, except for the larger charge sizes, a DSD formulation for PBX 9501 when calibrated to the slab geometry does not reproduce the corresponding diameter effect curve as closely as might be expected, given that PBX 9501 is an ideal explosive with a short reaction zone. On the other hand, a DSD formulation for PBX 9502 provides a significantly better representation of the size effect curve for equivalent values of the ratio of D_0 to the Chapman-Jouguet velocity[1]. There are a number of reasons for this. One possibility is an issue with the PBX 9501 experimental data. For instance, the rate-stick data only had one charge size (25.4-mm diameter) with associated front curvature data. Manufacturing of the small rate-stick charges could also be an issue, depending on whether the charges were pressed in molds or cut from large billets. The large HMX grains in PBX 9501 also can be an issue when machining to final diameter, where they can get easily pulled out of the explosive.

Another possibility for the break down of the DSD approach for PBX 9501 at smaller charge sizes is that high-order effects become important. These include front acceleration and transverse flow effects, which become relevant when order one changes in the shock angle across the charge are observed[15]. Figure 12 shows the shock angle across the various slab charges as a function of distance from the center of the slab, both for the exponential DSD fit form and also derived from the log-fit forms

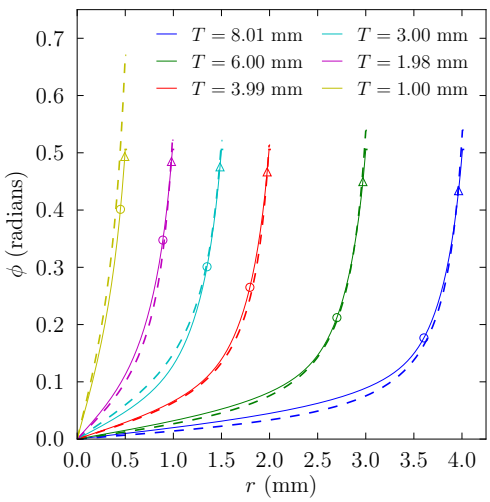

Fig. 12. Shock angle (ϕ) in radians vs r for the various slab tests. The DSD calculations (for the exponential functional form case) appear in solid lines and their experimental analogues derived from the log-form fits appear as dashed lines.

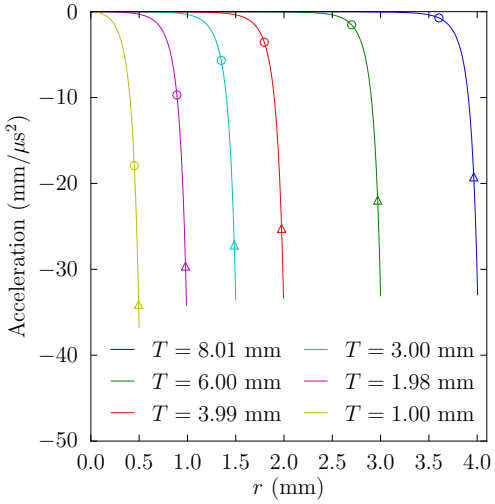

Fig. 13. Higher order DSD acceleration term $DD_n/Dt = -(D_0 \sin\phi)^2\kappa_s$ calculated for each slab test from the DSD calibration of the exponential functional form.

to the experimental data. Figure 13 shows the corresponding magnitude of the higher-order DSD acceleration term $DD_n/Dt = -(D_0 \sin\phi)^2\kappa_s$ based on the DSD exponential functional form. For the larger slab thicknesses, order one changes in ϕ and DD_n/Dt are only observed near the charge edge. However, for the smaller charges, the acceleration terms become large across a significant section of the charge, indicating that the phase velocities would likely be significantly influenced by higher-order effects.

References

1. Jackson, S. and Short, M., "Scaling of Detonation Velocity in Cylinder and Slab Geometries for Ideal, Insensitive and Non-Ideal Explosives," *J. of Fluid Mech.*, 2014, to appear.

2. Aslam, T. D., "Detonation shock dynamics calibration of PBX 9501," in "AIP Conf. Proc.", Vol. 955, p. 813, 2007.

3. Kapila, A. K., Bdzil, J. B. and Stewart, D. S., "On the structure and accuracy of programmed burn," *Combust. Theory Model.*, Vol. 10, pp. 289–321, 2006.

4. Bdzil, J. B., Stewart, D. S. and Jackson, T. L., "Program burn algorithms based on detonation shock dynamics: discrete approximations of detonation flows with discontinuous front models," *J. Comput. Phys.*, Vol. 174, pp. 870–902, 2001.

5. Bdzil, J. and Stewart, D., "Modeling two-dimensional detonations with detonation shock dynamics," *Phys. of Fluids A: Fluid Dyn.*, Vol. 1, p. 1261, 1989.

6. Bdzil, J. and Stewart, D., "The Dynamics of Detonation in Explosive Systems," *Ann. Rev. Fluid Mech.*, Vol. 39, pp. 263–292, 2007.

7. Bdzil, J., Fickett, W. and Stewart, D., "Detonation shock dynamics: A new approach to modeling multi-dimensional detonation waves," in "Ninth Symposium (Int.) on Detonation," pp. 730–42, 1989.

8. Stewart, D. S. and Bdzil, J. B., "The shock dynamics of stable multidimensional detonation," *Combust. Flame*, Vol. 72, pp. 311–323, 1988.

9. Aslam, T. D., Bdzil, J. B. and Stewart, D. S., "Level set methods applied to modeling detonation shock dynamics," *J. Comput. Phys.*, Vol. 126, pp. 390–409, 1996.

10. Cambell, A. and Engelke, R., "The Diameter Effect in High-Density Heterogenous Explosives," in "Proceedings of the 6th International Symposium on Detonation," pp. 642–652, Office of Naval Research, 1976.

11. Gibbs, T. and Popolato, A., *LASL Explosive Property Data*, pp. 234–249, University of California Press, 1980.

12. Hill, L., "Private communication," 2007.

13. Catanach, R. A. and Hill, L. G., "Diameter Effect Curve and Detonation Front Curvature Measurements for ANFO," in "Shock Compression of Condensed Matter," pp. 906–909, American Institute of Physics, 2001.

14. Skidmore, C., Phillips, D. and Howe, P., "The evolution of microstructural changes in pressed HMX explosives," *Technical Report LA-UR-97-2633*, Los Alamos National Lab., NM (United States), 1998.

15. Bdzil, J. B., Aslam, T. D., Catanach, R. A., Hill, L. G. and Short, M., "DSD front models: non-ideal explosive detonation in ANFO," in "12th Int. Det. Symp.", 2002.

Question

Michael L. Hobbs, SNL
What were your reasons for choosing the different fit forms, e.g. rational polynomial, exponential, etc.?
Reply by *Carlos Chiquete*

The idea was to show that the relatively poor prediction of the diameter effect data from the slab-based calibration was not a product of using a particular fitting form.

Question

John Bdzil, LANL
9501 - I see that the 2-to-1 radius-to-thickness scaling for the diameter-effect curve works well for 9501. Yet, you are showing that the two components of curvature are different. How is this explained?
Replies by *Carlos Chiquete*

This is the primary subject of our future investigation. As mentioned in our conclusions, the failure of the leading order $D_n - \kappa$ calibration to reproduce the relationship between the two size effect curves for the smaller charge sizes could be explained by the omission in the theory of front acceleration and transverse flow effects which are accentuated for these smaller tests. Alternatively (but more speculatively), problems in the data set itself could account for the discrepancy between theory and experiment.

9502 - Did you see the 2-to-1 scaling for 9502 for the diameter/slab effect?

The 2-to-1 scaling is not observed for PBX 9502 to the degree that it is for the PBX 9501 experimental data (See Jackson and Short[1]).

Given that you don't see the 2-to-1 scaling for the diameter/slab effect, how does DSD do at predicting the diameter/slab effect data given only the slab calibration results?

A calibration of the available slab data for PBX 9502 has not yet been performed, however, the rate-stick test based calibration is successful in reproducing the experimental slab geometry data according to Jackson and Short[1]. In relation to PBX 9502, it should be pointed out that the PBX 9501 calibration calculations require a greater departure in normal detonation velocities from D_{CJ}. DSD theory is derived under the assumption of *small* departures of the detonation front velocity from the limiting Chapman-Jouguet velocity.